AL36 - Visualization of Anode Effect in High Temperature Transparent Aluminum Electrolysis Cell

Bingliang Gao[1], Hongkun Niu[2], Cong Wang[3] and Zhiwei Liu[4]
1. Full professor
2. Doctoral degree student
3. Doctoral degree student
4. Doctoral degree student
School of Metallurgy, Northeastern University, Shenyang, 110819, China
Corresponding author: blgao@mail.neu.edu.cn

Abstract

The aluminum smelting industry is an important emitter of greenhouse gases. In addition to the emission of CO_2 during normal operation, perfluorocarbons (PFCs) are generated when the Al_2O_3 concentration in the electrolyte falls below a certain critical level – a phenomenon referred to as ***anode effect***. It is important that the mechanism of anode effect formation is well-understood to devise means of mitigating its occurrence. In this paper, the anode effect occurring at an industrial grade carbon anode with an underside surface area of 50 cm^2 (10 cm × 5 cm) was observed in a high temperature transparent electrolytic cell operating at 940 °C. The visual observation of the phenomenon confirmed that the anode effect is caused by the formation of an intermediate, insulating CF_x film. No gas layer or large bubbles were observed during the anode effect. The sharp increase of the cell voltage is caused by the insulating nature of the intermediate continuous unbroken film formed on the anode.

Keywords: Aluminum electrolysis, Transparent aluminum electrolysis cell, Carbon anode, Anode effect, PFC emissions.

1. Introduction

Hall-Héroult process is the only industrial process for primary aluminum production since 1886. Under normal electrolysis conditions, CO_2 is mainly released from the carbon anode. Under perturbed conditions when the alumina concentration falls below a critical level, perfluorocarbons (PFCs) consisting mostly of CF_4 with small amounts of C_2F_6 are generated on the carbon anode, accompanied by a cell voltage rise from about 4 V to about 20—65 V within a short time. The phenomenon is referred to as anode effect (AE) [1-2].

PFCs are potent greenhouse gases (GHGs) with extremely long lifetimes in the atmosphere and with high global warming potentials (GWPs). For example, CF_4 has a lifetime of 50 000 years and GWPs at 6 500 times the equivalent of CO_2 [3].

Most interpretations of the anode effect available in the literature may be summarized as combination of three causes [2, 4-10]:

1) Excessive increase in the concentration overpotential caused by depletion of dissolved alumina ($Al_2OF_6^{2-}$) near the interface of the anode/electrolyte;
2) The formation of intermediate carbon fluoride (CF_x) on the anode because of discharge of fluorine-containing ions;
3) The formation of a blanketing layer of a gaseous phase underneath the anode caused by a change in wettability of the anode to the electrolyte, which blocks the anodic current flow path to the electrolyte, resulting in a sharp increase of cell voltage.

In this paper, a see-through electrolytic cell operating at 940 °C was used to observe the anode effect occurring on an industrial grade carbon anode in a molten solution of Na_3AlF_6-AlF_3-LiF-CaF_2-Al_2O_3.

2. Experimental

Electrolyte (molar ratio of NaF/AlF_3 = 2.2) used in the experiment was a mixture of NaF (45.6 wt%), AlF_3 (41.4 wt%), CaF_2 (5 wt%), Al_2O_3 (3 wt%), LiF (5 wt%), which has a liquidus temperature of 920.9 °C. All chemicals were dried at 400 °C for more than 4 hours before use. The total weight of electrolyte used during the electrolysis experiments was 0.5 kg. Industrial anode material was used during the electrolysis experiments. The graphite cathodes were fabricated using high-purity graphite (Purity 99 %) by Kejin Graphite Ltd, Shenyang China. The industrial grade carbon anode was sampled from an aluminum smelter in China.

A high temperature see-through electrolysis cell was used for studying the phenomenon of anode effect occurring in the cryolite-based melt. The specific experimental details can be found in reference [11]. Here, a brief description of the experimental details will be provided. A high temperature see-through electrolysis cell, as shown in Figure 1, consists of a three-chamber quartz crucible with a middle chamber as the anodic compartment and two side chambers as the cathodic compartments (5). The entire crucible is held inside an electric furnace (3) with a bottom-observation window (7) and a side-observation window (10). There is also provided an image recording system (9), a data collecting system (8), and a 200 A DC power supply (1). There is a gap (2 mm high) between the quartz separating wall and bottom of the crucible, acted as a tunnel for bath flow and DC current flow between chambers. The carbon anode measures 100×50×70 mm, with the underside working surface area of 50 cm^2. Two graphite cathodes, each measures 50×12×70 mm, provide a total underside surface area of 12 cm^2. The current density of anode (ACD) applied was in the range of 0.3-1.5 A/cm^2 with intervals of 0.6 A/cm^2. Industrial carbon anode was electrolyzed for about 20 minutes at different current densities.

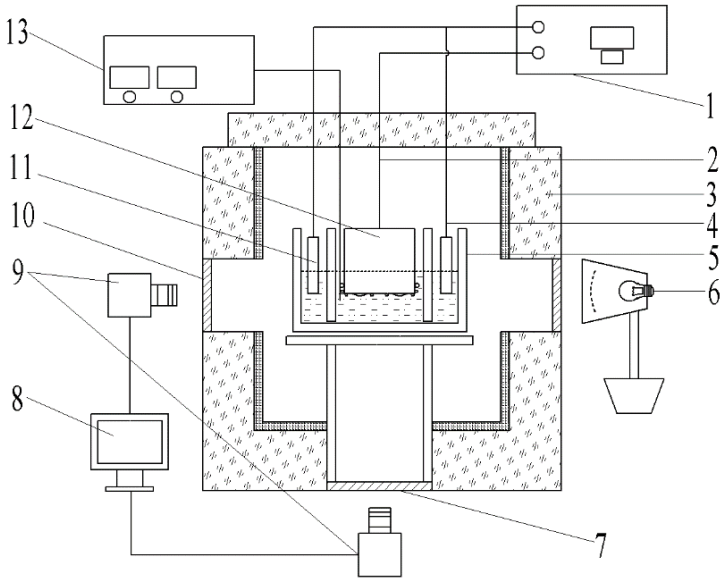

Figure1. Schematic diagram of the high temperature see-through aluminum electrolytic cell set-up.

1- 200 A DC power supply; 2- Anode current collecting rod; 3- Electric furnace; 4- Cathode current collecting rod; 5- Three-chamber quartz crucible; 6- Light source; 7- Bottom-observation quartz window; 8- Computer; 9- High speed camera; 10- Side-observation quartz window; 11- Graphite cathode; 12- Carbon anode; 13- Temperature controller.

3. Results and Discussion

3.1 Anode Voltage Oscillation and the Characteristic Bubble Morphologies

In this work, the bubble behavior at an industrial carbon anode was observed in the high temperature see-through electrolysis cell. Figure 2 shows the cell voltage profiles of electrolysis at Anode Current Densities (CD_{anode}) of 0.3, 0.9, 1.5 A/cm^2 (referred to as CI, CII and CIII in the Figure 2, respectively). For example, Figure 2 (b) shows the enlarged details of the voltage curve of the industrial carbon anode at CD_{anode} of 0.3 A/cm^2.

The cell voltages recorded at various CD_{anode} ranged from 5.3 V to 29.6 V, which is significantly greater than the normal cell voltage value, 4-5 V, as reported in the literature. The cell voltage components of the see-through electrolysis cell at various CD_{anode} were interpreted by the models suggested by Haupin, et al. [12] and listed in Table 1. Because of the large voltage drop through the chamber-separator gaps in the see-through cell and the large bath overvoltage between anode and cathode (see Table 1), it is reasonable for the value of the cell voltage to be in the range from 5 V to 20 V at the investigated range of CD_{anode} in this see-through electrolysis cell.

There was a sharp increase in cell voltage from 6.198 V to 29.650 V when the CD_{anode} adjusted from 0.3 A/cm^2 to 1.5 A/cm^2, which is much higher than the estimated value of 20.193 V at 1.5 A/cm^2 (see Table 1, assuming C_{Al2O3} = 3 %). The sharp increase of cell voltage is clearly a classical symptom of an anode effect.

As illustrated in Figure 2(b) and (c), the cell voltage fluctuation wave caused by the release of large bubbles was in the range of 150-290 mV at the industrial carbon anode within the CD_{anode} range from 0.3 to 0.9 A/cm^2. As shown in Figure 3, the development and appearance of the bubbles on the 50 cm^2 anodes follow similar patterns as those observed on a smaller graphite anode (11cm^2) which has been described in our previous studies [13-14], that is, the process of gas molecular formation, bubble nucleation, bubble growth, bubble coalescence, and bubble release. The edge of the anode was always crowded with small bubbles which get released from the anode at a high frequency ranging from 0.4 to 0.5 Hz, while in the middle region of the anode, it was always covered with large bubbles which get released at a low frequency ranging from 0.05 to 0.1 Hz.

Table 1. Estimation of cell voltage components at various CD_{anode}s, T_{bath} = 940 °C.

CD_{anode}, **A/cm^2**	**0.3**	**0.9**	**1.5**
$CD_{cathode}$, **A/cm^2**	1.25	3.75	6.25
E_{equil}, V	1.184	1.184	1.184
E_{bc}, V	1.123	3.371	5.618
E_{ba}, V	0.517	1.550	2.583
E_{bg}, V	1.680	5.040	8.400
E_{bub}, V	0.090	0.286	0.481
η_{as}, V	0.399	0.510	0.562
η_{ca}, V	0.035	0.035	0.035
η_{cc}, V	0.052	0.091	0.109
E_{cell}, V	5.325	12.799	20.193

Note: CD_{anode} - anode current density; $CD_{cathode}$- cathode current density; E_{equil}- equilibrium potential; E_{bc}- bath overvoltage in cathodic chamber; E_{ba}- bath overvoltage in anodic chamber; E_{bg}- bath overvoltage through separator gap; E_{bub}- bubble overvoltage; η_{as}- surface overvoltage at anode; η_{ca}- concentration overvoltage at anode; η_{cc}- concentration overvoltage at cathode; E_{cell}- total cell voltage.

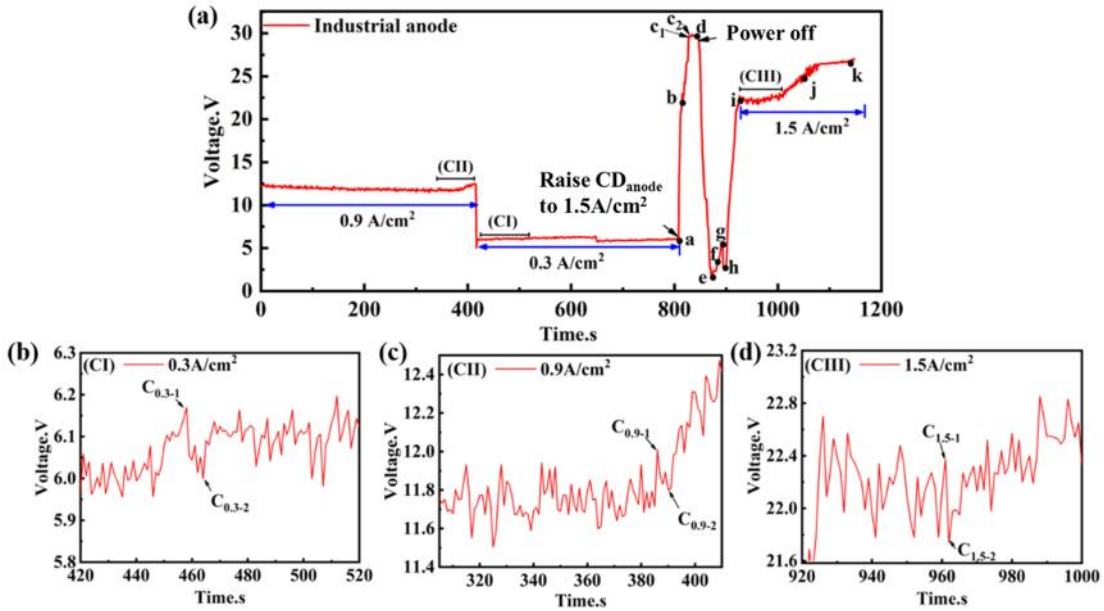

Figure 2. (a) cell voltage of electrolysis using industrial carbon anodes working at various CD_{anode}s; (b) cell voltage at CD_{anode} of 0.3 A/cm^2; (c) cell voltage at CD_{anode} of 0.9 A/cm^2; (d) cell voltage at CD_{anode} of 1.5 A/cm^2.

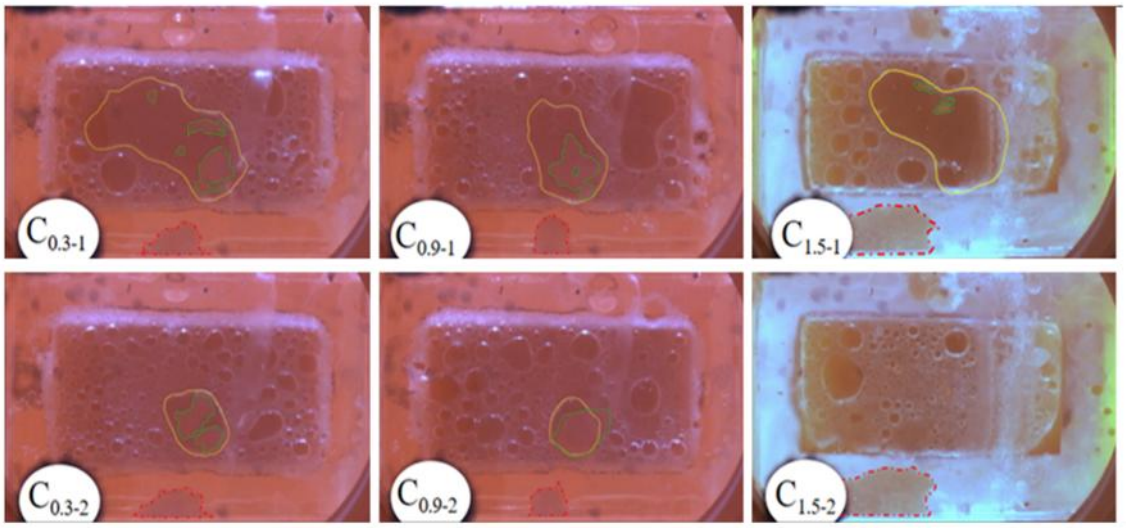

Figure 3. The bubbles profiles at the industrial carbon anode working at various anode current densities.

3.2 Anode Effect and CF_x Film

The photos in Figure 4 (also refer to Figure 2, points a, b, c1, c2, d, e) illustrate the process of the anode effect that occurred at the industrial carbon anode used. Figure 4 (a) shows the situation just before the anode effect with the anode operating at 0.3 A/cm^2. When the anode effect is initiated, it occurs first at the two short opposite edges of the anode, where the bubbles completely disappeared when the CD_{anode} was increased to 1.5 A/cm^2 from 0.3 A/cm^2, as shown in Figure 4 (b). Following this, the bubble-free area expanded very quickly from two short edges towards the center of the anode. 5 seconds later, as shown in Figure 4 (c1), a very bright explosion-like fire ball was observed at the center of the area coupled with the sound of an explosion when all bubbles

suddenly disappeared and with cell voltage very quickly rises to 29.6 V. Immediately following this, the whole anode bottom surface was covered with small bright sparks as shown in Figure 4 (c2). Then, most sparks disappeared, and some tiny sparks could also be observed at the top left corner of the anode as shown in Figure 4 (d). After turning off the power, as shown in Figure 4 (e) and Figure 2 (refers to point e), the sparks disappeared, and the cell voltage decreased to 1.66 V.

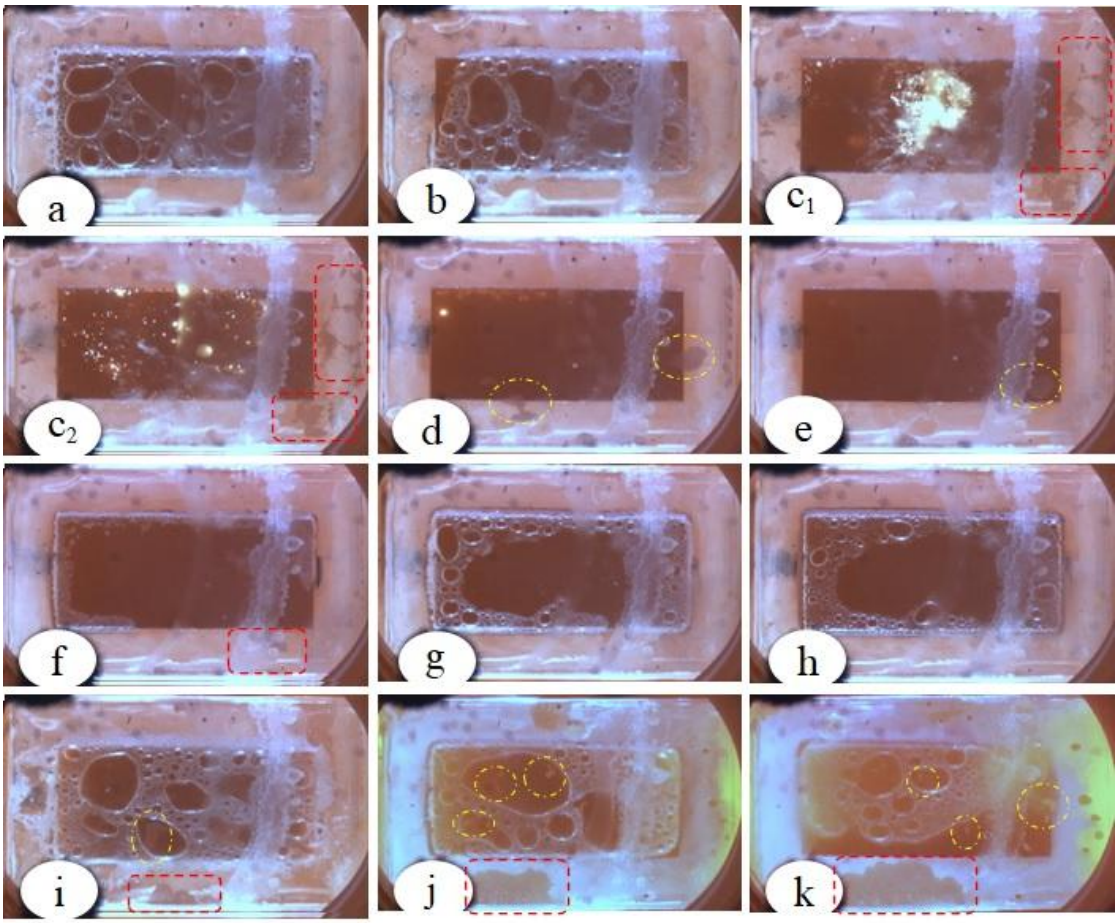

Figure 4. The process of the anode effect observed in high temperature see-through electrolysis cell.

During the anode effect, we did not observe any bubbles or persistent bubble layer blanketing the anode bottom surface. The widely accepted mechanism for anode effect, that a blanketing bubble layer blocks the current path and causes a sharp increase of the voltage, is clearly incorrect.

After the anode effect, the electrolysis was restarted at a CD_{anode} of 0.1 A/cm^2 (refers also to point f in Figure 2). Initially, small bubbles could only be observed around the edges of the anode, as shown in Figure 4 (f). Then, when the CD_{anode} was increased to 0.2 A/cm^2 (refers also to point g in Figure 2), within about 30 seconds, the anode bottom surface was covered with bubbles, which signifies the recovery of normal electrolysis, as shown in Figure 4 (g). Following this, the CD_{anode} was slowly increased to 1.5 A/cm^2, and the average cell voltage was about 22.2 V. As shown in Figure 4 (i) (refers also to point i in Figure 2), the anode was covered with large bubbles and patches of small foamy bubbles. About three minutes later, a bubble-free area initially appeared at the lower-right corner of the anode, which gradually spread to almost half the area of the anode before the electrolysis experiment was finished, as shown in Figure 4 (j) and (k). During this

period, the cell voltage increased up to 26.6 V. This therefore indicates that a second anode effect was beginning to occur, which exhibited a different behavior compared to the first one.

During the second anode effect, some bubbles or part of bubbles were obscured by some film-like formation, which could also be seen near the lower side of the anode and built up on the bottom of the crucible during electrolysis, see the areas marked using yellow and red dashed-lines in Figure 4 (i), (j) and (k). These films were formed at the anode and exfoliated as thin layers from the anode under the action of the moving bubbles. We can also find these exfoliated films near the anode during the first anode effect, see the areas marked with red dashed lines in Figure 4 (c1) and (c2). After checking the electrolysis videos of the industrial carbon anode at 0.3 A/cm^2 and 0.9 A/cm^2, such films could also be observed, as shown in Figure 3, marked with green dashed lines on bubble surface and red dashed lines in other areas. However, it must be noted that the existence of film in the 0.3 A/cm^2 electrolysis experiment should be the remains of film formed in the 0.9 A/cm^2 electrolysis because the film could not be observed at the end of the lower CD_{anode} electrolysis experiments.

The film observed to form is expected to be denser than the cryolite-based electrolyte because it was always found resting at the bottom of the crucible. The exfoliated film should not be considered as carbon layer, which is predicted to float on the surface of the cryolite-based molten salt because of its lower density compared to the cryolite solution. Luly [15] systematically studied the physical properties of fluorinated carbon black, which was prepared by the direct fluorination of carbon black with fluorine. The densities of the CF_x with %fluorine = 10 % ($CF_{0.07}$), 28 % ($CF_{0.25}$) and 65 % ($CF_{1.16}$) are 1.9 g/cm^3, 2.1 g/cm^3 and 2.5 g/cm^3, respectively [15]. The density of the molten salt used in this experiment is estimated as 2.067 g/cm^3 based on the experimental density equation for the cryolite-based electrolyte suggested by Kvande [16]. Therefore, the formed CF_x film observed in this experiment should have %fluorine of about 28 % at least and x value of about 0.25 higher. The corresponding resistivity of the $CF_{0.25}$ is about 1.1×10^{10} Ω·cm, which increases with x in the CF_x [15]. The sharp increase of the cell voltage is clearly caused by the insulating nature of the CF_x.

Some studies [15-18] have confirmed that the intermediate carbon monofluoride compound decomposes to CF_4 and C_2F_6 at the temperature above 600 ℃. The thermodynamical decomposition temperature of $CF_{0.25}$ and $CF_{1.2}$ is about 450 ℃ and 500 ℃, respectively [15]. Based on our observations, the decomposition rate was not fast. For example, after the second anode effect, the built-up films in the melt disappeared completely in about 50 s.

Luly [15] stated that fluorine preferentially attacks the carbon atoms at the less graphitic regions. Consequently, some discrete islands with relatively high fluorine concentrations are formed on the carbon material, whose fluorine concentrations depend only on their depth from the surface. As x of the CF_x increases, these islands merge to yield a completely fluorinated crust, or film on the surface of the carbon substrate [15].

In a normal Hall-Héroult aluminum electrolysis cell, the liquid aluminum cathode is considered as the actual cathode and is directly under the anode. The dissolved aluminum diffuses into the molten salt and reacts with exfoliated carbon fluoride film to result in the product of carbon and AlF_3. Therefore, it is very difficult to find and collect the remains of this insulating film after the electrolysis.

The very bright fire ball explosion is due to an electrical arc generated though the high electrical resistance film layer on the anode carbon surface. Electrical current will eventually find a way to be conducted in the cell as the voltage potential increases significantly across the higher resistance film layer. The small sparks are also due to electrical arcs on small individual pieces of the film.

4. Conclusion

In this work, a see-through high temperature cell was used to study the bubble behavior at an industrial carbon anode at anodic current densities ranging from 0.3 to 1.5 A/cm^2. The phenomenon of anode effect at an industrial carbon anode was observed when the current density of anode was 1.5 A/cm^2.

During the anode effect, no bubbles or persistent bubble layer blanketing the anode bottom surface was observed. We did observe the growth of a bubble-free area accompanied by a 'fire-ball' type of explosion and a loud noise. The exfoliated films during the anode effect were observed and considered as CF_x with value of x greater than 0.25 based on its density evaluation. CF_x has very high resistivity and contributes to the sharp rise of the cell voltage. Due to the insulation of the CF_x film at the fluorinated area, it will cease both the oxidation of oxygen ions and bubble formation. Therefore, bubble-free area starts growing and expands eventually. Hence, working area of the anode decreases, which promotes fluorination of carbon atoms and initiates anode effect. It confirms that the anode effect is caused by the formation of intermediate insulating CF_x film.

5. References

1. Alton T. Tabereaux, Anode effects, PFCs, global warming, and the aluminum industry, *JOM*, 1994, 46(11), 30-34.
2. Warren Haupin and Edward J. Seger, Aiming for zero anode effects, *Light Metals* 2001, 767-773.
3. Eric Jay Dolin, PFC emissions reductions: the domestic and international perspective, *Light Metal Age-CHICAGO-*, 1999, 57, 56-67.
4. David S. Wong et al., PFC emissions from detected versus nondetected anode effects in the aluminum industry, *JOM*, 2015, 67, 342-353.
5. J. Thonstad, F. Nordmo and K. Vee, On the anode effect in cryolite-alumina melts-I, *Electrochimica Acta*, 1973, 18(1), 27-32.
6. J. Thonstad, F. Nordmo and J. K. Rødseth, On the anode effect in cryolite-alumina melts-II the initiation of the anode effect, *Electrochimica Acta*, 1974, 19(11), 761-769.
7. H. Vogt, On the mechanism of the anode effect in aluminum electrolysis, *Metallurgical and Materials Transactions B*, 2000, 31, 1225-1230.
8. H. Vogt, On the various types of uncontrolled potential increase in electrochemical reactors-The anode effect, *Electrochimica acta*, 2013, 87, 611-618.
9. H. Vogt, The anode effect as a fluid dynamic problem, *Journal of applied electrochemistry*,1999, 29, 137-145.
10. Zhu-xian Qiu and Ming-jie Zhang, Studies on anode effect in molten salts electrolysis, *Electrochimica acta*, 1987, 32(4), 607-613.
11. Bing-liang Gao et al., Visualization of Anode Effect in Aluminum Electrolysis*, Journal of The Electrochemical Society*, 2022, 169(1), 013505.
12. Warren Haupin, Interpreting the components of cell voltage, *Light Metals* 2016, 153-159.
13. Zhi-bin Zhao et al., Observation of anodic bubble behaviors using laboratory scale transparent aluminium electrolysis cells, *Light Metals* 2015, 801-806.
14. Zhi-bin Zhao et al., Anodic bubble behavior and voltage drop in a laboratory transparent aluminum electrolytic cell, *Metallurgical and materials Transactions B*, 2016, 47, 1962-1975.
15. Matthew H. Luly, Electrical resistivity of fluorinated carbon black, *Journal of Materials Research*, 1988, 3(5), 890-897.
16. Halvor Kvande, The structure of alumina dissolved in cryolite melts, *Light Metals* 1986, 96-104.

17. Gong Chen et al., Electrochemical behavior of graphite anode during anode effect in cryolite molten salts, *Transactions of Nonferrous Metals Society of China*, 2012, 22(9), 2306-2311.
18. A.K. Kuriakose and J.L. Margrave, Kinetics of the reactions of elemental fluorine. IV. Fluorination of graphite, *The Journal of Physical Chemistry*, 1965, 69(8), 2772-2775.